Nano Energy 80 (2021) 105542

Contents lists available at ScienceDirect

Nano Energy

journal homepage: http://www.elsevier.com/locate/nanoen

Full paper

Metal-organic layers as a platform for developing single-atom catalysts for photochemical CO_2 reduction

Ji-Hong Zhang [a,1], Wei Yang [a,1], Min Zhang [a], Hong-Juan Wang [a,*], Rui Si [b,*], Di-Chang Zhong [a,*], Tong-Bu Lu [a]

[a] Institute for New Energy Materials and Low Carbon Technologies, School of Materials Science and Engineering, Tianjin University of Technology, Tianjin 300384, China
[b] Shanghai Synchrotron Radiation Facility, Shanghai Institute of Applied Physics, Chinese Academy of Sciences, Shanghai 201204, China

ARTICLE INFO

Keywords:
Metal-organic layers
Carbon nitride
Photochemical CO_2 reduction
Single-atom cobalt catalyst
Metal-organic frameworks
MOF nanosheets

ABSTRACT

The photochemical reduction of carbon dioxide (CO_2) into valuable chemicals or feedstock is very meaningful for environmental and energy sustainability. Development of efficient, robust and low-cost catalysts is necessary and desirable for their practical application. In this communication, we exploited such a catalyst by anchoring single-Co(II) sites on g-C_3N_4, which was firstly achieved by the pyrolysis of ultrathin cobalt metal-organic framework (MOF) nanosheets (also called metal-organic layers; MOLs) during the process of g-C_3N_4 formation. Benefitting from the confinement effect of MOL matrix and the close contact between MOLs and g-C_3N_4 precursor, the Co(II) sites can be homogeneously and atomically dispersed on the surface of g-C_3N_4 during the process of g-C_3N_4 formation. Impressively, this photocatalyst possesses excellent catalytic performance for photochemical CO_2-to-CO conversion, with the CO evolution rate as high as 464.1 μmol g^{-1} h^{-1}, 3 and 222 times higher than those of using bulky Co-MOF and $CoCl_2$ as the cobalt sources, respectively. This work paves a new way to develop the cost-effective photocatalysts containing single-atom sites for clean energy production.

1. Introduction

It is well-known that the excessive emission of greenhouse gas carbon dioxide (CO_2) will eventually destroy the carbon balance and trigger many serious environmental problems [1,2]. Inspired by the natural photosynthesis of green plants, researchers conceived an ideal approach to solve these problems, that is, using clean and abundant solar energy to drive the catalytic reduction of CO_2 to value-added chemical products [3–13]. This approach could kill two birds with one stone, as it can not only address the environmental problem, but also solve the coming energy crisis. The key point must be addressed wherein is the building of efficient catalytic systems like chloroplasts. During past several decades, many photochemical systems have been constructed to convert CO_2 into CO [14–17], CH_4 [18–22], HCOOH [23,24], and other hydrocarbons [25–28]. However, for those systems with high catalytic efficiency, noble metals in catalysts or photosensitizers are indispensable [29], which limits them toward widespread application, and the valid solutions are still urgently needed.

Recently, many endeavors have been devoted to the development of cost-effective catalytic systems without any noble metals [30–32]. In this regard, graphitic carbon nitride (g-C_3N_4), a kind of fascinating metal free polymeric semiconductor, has emerged as a promising photocatalyst owing to its visible-light response, non-toxic, high stability, as well as low-cost and facile synthesis [33–37]. A large number of g-C_3N_4-based catalysts have been widely explored in photocatalytic degradation of toxic environmental pollutants [38,39], as well as photochemical energy storage and conversion [40,41]. However, due to the insufficient visible light utilization and rapid recombination of photogenerated carriers, the efficiency of pure g-C_3N_4 for these reactions is far from satisfaction [42]. Apart from combining g-C_3N_4 with other semiconductors to overcome these problems [43–48], anchoring metals atomically on the surface of g-C_3N_4 is considered as a more facile and effective approach, by which the light absorption range can be extended, the separation efficiency of photogenerated carriers can be improved, and the surface catalytic reaction kinetics can be accelerated [49–52]. At present, several methods have been proved to be capable of loading single atoms on g-C_3N_4, such as wet chemical route [52,53], atomic layer deposition [54] and thermal copolymerization [55,56]. However,

* Corresponding authors.
E-mail addresses: hongjuanwang@tjut.edu.cn (H.-J. Wang), sirui@sinap.ac.cn (R. Si), zhong_dichang@hotmail.com, dczhong@email.tjut.edu.cn (D.-C. Zhong).
[1] These authors contributed equally to this work.

https://doi.org/10.1016/j.nanoen.2020.105542
Received 24 September 2020; Received in revised form 17 October 2020; Accepted 21 October 2020
Available online 1 November 2020

the preparation of g-C_3N_4-based single atom catalysts with high-loading single atoms is still a crucial challenge, due to the nucleation and crystal growth.

Spatial confinement to metal centers in precursors could be an effective strategy to prevent single metal ions from agglomerating through limiting their diffusion. In this regard, metal-organic framework (MOF) nanosheets (also called metal-organic layers; MOLs), with exposed active sites orderly confined on the nanosheet surface [57–65], would be ideal metal-source precursors to prepare g-C_3N_4-based photocatalysts. In this communication, we first of all prepared a type of Co-MOLs from a 3D layer-pillared bulky Co-MOF $\{[Co_3(IDC)_2(4,4'\text{-bipy})_3]\cdot 6\ H_2O\cdot DMF\}_n$ [66] in large scale by our recently developed ligand replacement approach [67], that is, the pillars (4,4′-bipyridine) of the 3D Co-MOF were replaced by terminal dimethyl sulfoxide (DMSO) solvent molecules (Scheme 1). Then we aimed to establish a close linkage between Co-MOLs and semiconductor g-C_3N_4, to tentatively prepare efficient and cheap catalysts for photochemical CO_2 reduction (Scheme 1). The linkage was achieved by pyrolysis of ultrathin 2D Co-MOLs during the preparation of g-C_3N_4 using urea as a precursor, wherein, the Co(II) sites in the MOL matrix could be transferred and anchored on the g-C_3N_4 ultrathin layer. As a result, the confinement effect of MOLs can effectively prevent the diffusion of cobalt atoms during the pyrolysis process, producing a g-C_3N_4-based photocatalyst with high loading and highly-dispersed single Co(II) sites. This photocatalyst, integration of catalyst and photosensitizer, exhibits much high performance for photocatalytic CO_2-to-CO conversion in CH_3CN/H_2O. The CO generation rate can reach up to 464.1 $\mu mol\cdot g^{-1}\cdot h^{-1}$, which is 3 and 222-fold than those using bulky Co-MOF and $CoCl_2$ as the cobalt sources, respectively.

2. Results

2.1. Preparation and characterization

The bulky Co-MOF $\{[Co_3(IDC)_2(4,4'\text{-bipy})_3]\cdot 6\ H_2O\cdot DMF\}_n$ was synthesized by solvothermal method according to the literature method [66], which was characterized by powder X-ray diffraction (XRD, Fig. S1) and scanning electron microscope (SEM, Fig. S2), and then used for the following MOL preparation. The as-prepared bulky Co-MOF crystals were dispersed in dimethyl sulfoxide (DMSO) and continuously ultra-sonicated for 10 h at room temperature. The pillar 4,4′-bipyridine ligands in bulky Co-MOF were gradually replaced by terminal DMSO, resulting in ultrathin Co-MOLs highly-dispersed in the DMSO solution (Scheme 1). During the exfoliation process, a remarkable color change of the mixture from orange turbid to pink clear was detected, and a typical Tyndall effect was observed (Fig. 1a and b). These observations preliminarily illustrate the formation of MOLs.

The infrared spectrum (IR) of Co-MOLs shows that a new peak appears at 1043 cm^{-1} in contrast to that of bulky Co-MOF (Fig. S3). This new peak corresponds to the -S=O stretching vibration of DMSO, indicating that the DMSO molecules have replaced 4,4′-bipyridine in 3D bulky Co-MOF to afford 2D MOLs. Thermogravimetric analyses (TG) demonstrated the slightly decreased thermal stability of the Co-MOLs compared with the bulky Co-MOF (Fig. S4), which can be attributed to the easy loss of the terminal DMSO than the pillared bridge 4,4′-bipyridine. Powder XRD results show that the diffraction peaks of Co-MOLs are noticeably less than those of the bulky Co-MOF. The peaks at 8.1, 16.1, and 24.0° correspond to the crystal faces with Miller indices of (100), (200) and (300) (Fig. S5). The equidistance of these diffraction peaks demonstrates that the Co-MOLs with layered structure have been successfully prepared. Scanning electron microscopy (SEM) was further used to screen the micro-morphology of the Co-MOLs. As shown in Fig. 1c and d, very thin and free-standing nanosheets were observed, with a lateral size of hundreds of nanometers to several micrometers. To obtain the exact thickness, the Co-MOLs highly-dispersed in ether solution were laid on a mica plate and measured by atomic force microscopy (AFM). The AFM analyses clearly showed that the Co-MOLs have uniform thickness of ~1.5 nm, corresponding to the single layer MOL simulated from the crystal structure (Fig. 1e and Fig. S6). In all, all above results evidence that 2D ultrathin Co-MOLs have been successfully prepared from the 3D bulky counterpart, and solidly illustrate that the ligand replacement approach is general for producing 2D MOLs from 3D MOFs [67].

The as-prepared 2D ultrathin Co-MOLs were used as cobalt resources for synthesizing g-C_3N_4. Four types of g-C_3N_4-based catalysts were prepared by pyrolysis of 5.0 g urea precursor at 550 °C under air using 10, 20, 30 and 40 mg Co-MOLs as cobalt resources, respectively (The obtained catalysts were designated as g-C_3N_4-MOLs-X; X represents the amount of Co-MOLs used). The resulting g-C_3N_4-MOLs-X catalysts were collected and used for subsequent morphology characterization and photochemical CO_2 reduction.

Powder XRD patterns show that the matrix of g-C_3N_4 has not changed after the in situ incorporation of Co(II) ions (Fig. S7). No peak assignable to cobalt oxide was observed. This observation shows that the structures of g-C_3N_4-MOLs-X catalysts are similar to that of g-C_3N_4, and the Co(II) ions were highly distributed on g-C_3N_4 matrix. The inductively coupled plasma mass spectrometer (ICP-MS) results demonstrate that with the increase of the amount of Co-MOLs used, the cobalt contents in the resulting catalysts increase (Table S1). Transmission electron microscopy (TEM) shows that the morphology of g-C_3N_4-MOLs-30 assumes sheet structure. No cobalt oxide nanoparticle or nanocluster was observed, consistent with the XRD results (Fig. 2a). The element mappings further confirm the uniform dispersion of C, N and Co in g-C_3N_4-MOLs-30 (Fig. 2b). The high-angle annular dark field scanning transmission electron microscopy (HAADF-STEM) images display abundant bright dots, as highlighted by the circles in Fig. 2c and d. These bright dots correspond to the heavy Co sites homogeneously implanted in g-C_3N_4 nanosheets. The electronic structure and short-range coordination environment of Co site were further examined by X-ray absorption near-edge structure (XANES) and extended X-ray absorption fine structure (EXAFS). As depicted in Fig. 2e, Co K-edge XANES spectra show that the absorption energy of g-C_3N_4-MOLs-30 is similar to that of the CoO standard, revealing that the valence of Co^{2+} in g-C_3N_4-MOLs-30. It should be noted that the XANES profile of g-C_3N_4-MOLs-30 is slightly different from that of CoO, indicating that the coordination environments

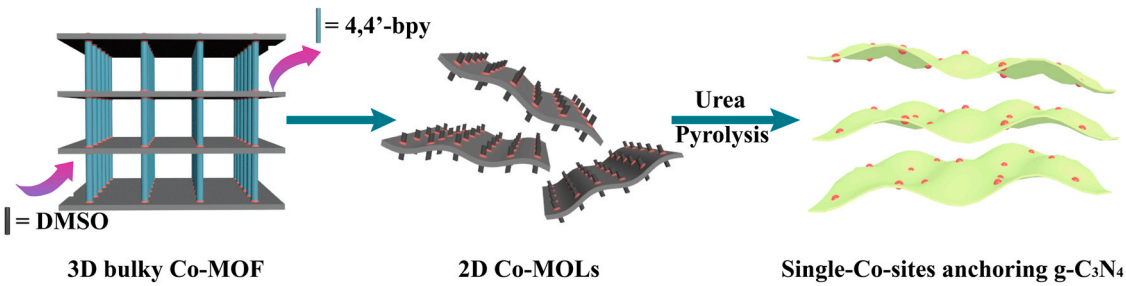

Scheme 1. Schematic diagram showing the preparation process of single-Co-sites anchoring g-C_3N_4-MOLs.

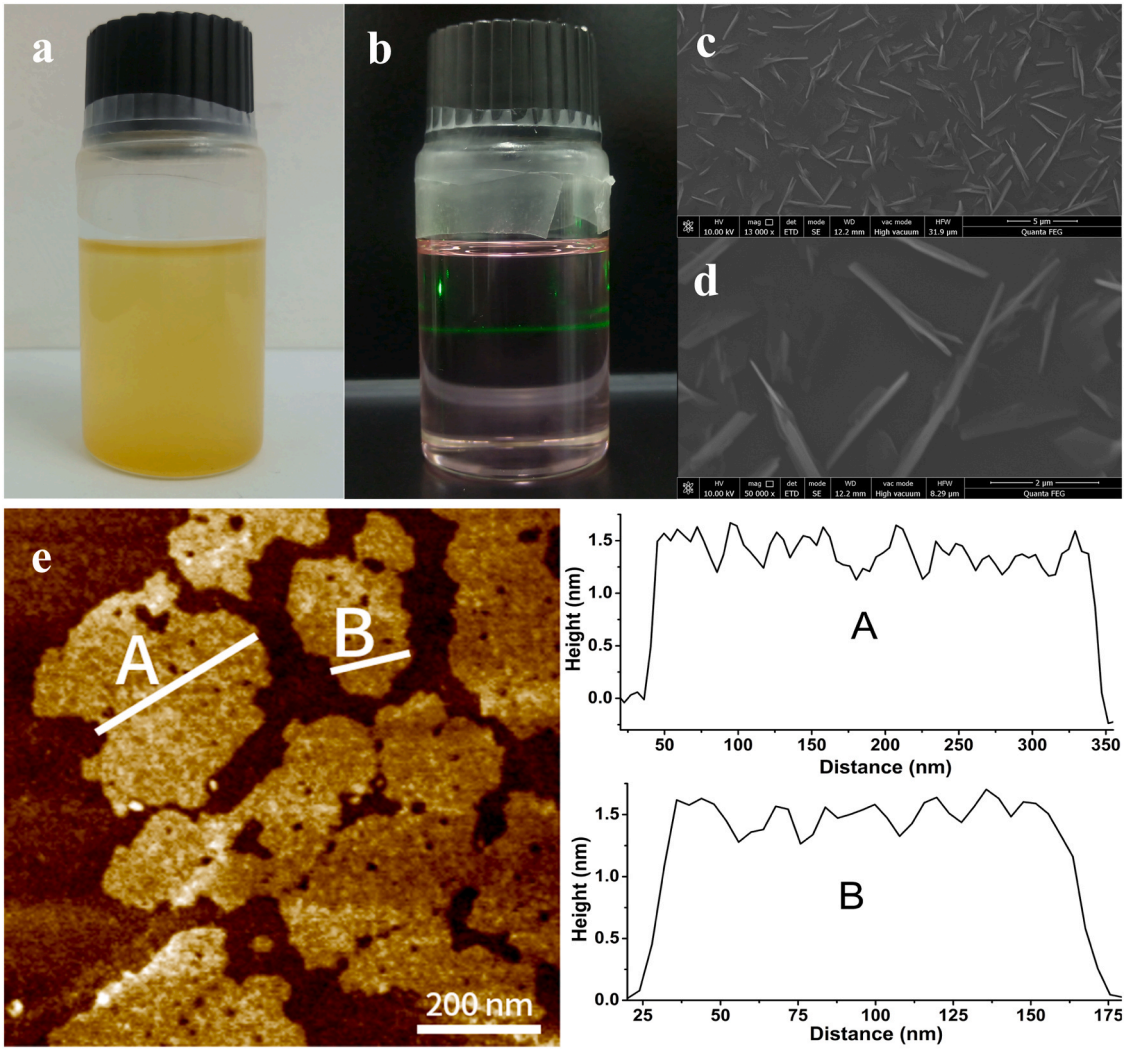

Fig. 1. Preparation and characterization of Co-MOLs. a, bulky Co-MOF dispersed in DMSO. b, bulky Co-MOF in DMSO after ultrasound for 10 h, resulting a clear solution with Tyndall effect, indicative of the formation of Co-MOLs. **c** and d, SEM images of Co-MOLs. e, AFM image and corresponding thickness of Co-MOLs.

of Co(II) in g-C_3N_4-MOLs-30 is different from that in CoO. The EXAFS spectrum of R space for g-C_3N_4-MOLs-30 exhibits a main peak around 1.84 Å, slightly shorter than Co–O (1.99 Å) in CoO, indicating that the Co(II) in g-C_3N_4-MOLs-30 may be coordinated by N atoms (Fig. 2f). This was confirmed by the fitting result. As shown in Fig. S8, the Co–N fitting curve accords well with the experimental curve, further evidencing N atoms around Co(II) in g-C_3N_4-MOLs-30. In addition, the peak at about 2.45 Å corresponding to Co–Co is absent, revealing the isolated dispersion of Co(II) on g-C_3N_4-MOLs-30, which is consistent with the HAADAF-STEM result. X-ray photoelectron spectroscopic (XPS) measurements were further carried out for g-C_3N_4-MOLs-30. As shown in Fig. S9, the survey spectrum presents the elemental peaks of Co, C, N and O, consistent with the results of EDX mapping (Fig. S10). Specifically, the Co 2p high-resolution spectrum shows two main characteristic peaks at 797.2 and 782.0 eV, and two fitted satellite peaks at 803.5 and 786.2 eV, corresponding to the binding energy of Co $2p_{1/2}$ and Co $2p_{3/2}$, respectively (Fig. S9b). These observations suggest Co^{2+} species in g-C_3N_4-nanosheets-30 [68]. Furthermore, according to the references [69], the strong peaks centered at 782.0 eV originated from the chemical bonding between Co and N, which confirms the existence of Co@N_x species in g-C_3N_4-MOLs-30. The N atoms present different chemical states in g-C_3N_4-MOLs-30 (Fig. S9c). The N 1 s signals at 398.7, 399.2, 401.0 and 404.6 eV correspond to pyridinic N (398.6 eV), Co–N (399.2 eV), graphitic N (401.0 eV) and oxide N (404.6 eV), respectively. The above results reveal that the single Co sites were homogeneously atomically dispersed on g-C_3N_4. It is worth noting that in g-C_3N_4-MOLs-30, the Co content reaches as high as 1.72% (Table S1), much higher than those of reported g-C_3N_4-based single-metal-site catalysts prepared by the conventional wet chemical route [52,53,70,71], which demonstrates that the co-pyrolysis of MOLs and urea is an improved approach for preparation of g-C_3N_4-based single-metal-site catalysts.

2.2. Photocatalytic CO_2 reduction

The experiments on photocatalytic CO_2 reduction by g-C_3N_4-MOLs-X were performed in a CH_3CN/H_2O/TEOA solution. Typically, a glass reactor containing a mixture of 5 mL CO_2-saturated CH_3CN/H_2O/TEOA (*v:v:v* = 3:1:1) and g-C_3N_4-MOLs-X was irradiated by a 300 W Xe lamp with wavelengths over 420 nm. The generated gases were analyzed by a gas chromatography and the liquid products were detected by an ion chromatography. As shown in Table 1, g-C_3N_4-MOLs-X catalysts show good activity for photochemical CO_2 reduction, generating a large amount of CO and a small amount of H_2. No liquid product was detected. With the increase of Co-MOLs from 10 to 30 mg, the amount of CO generated remarkably increases (Table 1, Entry 1–3). Further increase the amount of Co-MOLs to 40 mg, the amount of CO generated decreases (Table 1, Entry 4). These observations indicate that 30 mg Co-MOLs is the proper amount used as cobalt sources to prepare single-Co-sites

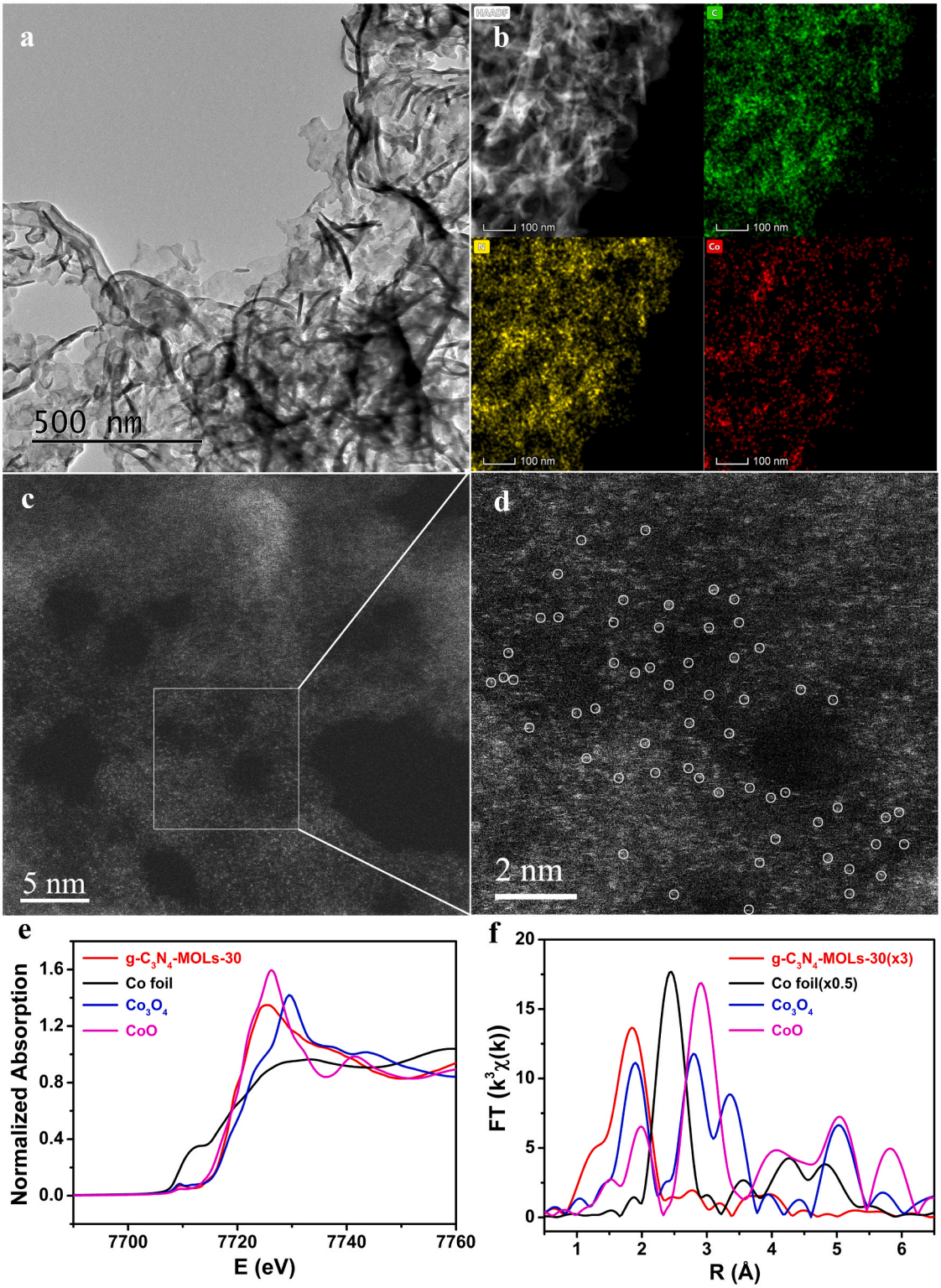

Fig. 2. Morphology and composition of g-C_3N_4-MOLs-30. a, TEM image of g-C_3N_4-MOLs-30. b, EDX elemental mapping of g-C_3N_4-MOLs-30. c and d, HAADF-STEM images of g-C_3N_4-MOLs-30. e, Co K-edge XANES profiles for g-C_3N_4-MOLs-30, Co foil, Co_3O_4 and CoO. f, Co K-edge k^3-weighted FT-EXAFS spectra of g-C_3N_4-MOLs-30, Co foil, Co_3O_4 and CoO.

depositing g-C_3N_4 catalyst. With 2.0 mg g-C_3N_4-MOLs-30, 9.28 μmol CO and 1.85 μmol H_2 were produced in 10 h, corresponding to the CO generated rate of 464.1 $\mu mol \cdot g^{-1} \cdot h^{-1}$ and the CO selectivity of 83.4% (Fig. 3a; Table S2). To our knowledge, the CO evolution rate exceeds many reported C_3N_4-based photocatalysts (Table S3). Under the same conditions, when the CO_2 was replaced with Ar, no CO was detected (Table 1, Entry 5), illustrating that the CO was originated from the CO_2 reduction. To further confirm this conclusion, the isotope labeling $^{13}CO_2$ was used instead of CO_2. As shown in Fig. S11, a peak with *m/z* value of 29 corresponding to ^{13}CO appears, directly evidencing that the CO was generated from the CO_2 reduction. Control experiments were also carried out without catalyst, TEOA or illumination. In these cases, no CO

Table 1
The results of photocatalytic reduction of CO_2 to CO by different catalysts under the same conditions[a].

Entry	Catalyst	CO ($\mu mol \cdot g^{-1}$)	H_2 ($\mu mol \cdot g^{-1}$)	CO ($\mu mol \cdot g^{-1} \cdot h^{-1}$)	CO (%)
1	g-C_3N_4-MOLs-10	202.6	49.5	20.3	80.4
2	g-C_3N_4-MOLs-20	1825.2	207.0	182.5	89.8
3	g-C_3N_4-MOLs-30	4640.8	926.2	464.1	83.4
4	g-C_3N_4-MOLs-40	3317.6	564.8	331.7	85.5
5 [b]	g-C_3N_4-MOLs-30	0	110.2	0	0
6[c]	–	0	0	0	0
7[d]	g-C_3N_4-MOLs-30	0	0	0	0
8[e]	g-C_3N_4-MOLs-30	0	0	0	0
9	g-C_3N_4	0	0	0	0
10	Co-MOLs	0	0	0	0
11	g-C_3N_4&Co-MOLs	356.3	321.7	35.6	52.6
12	g-C_3N_4&$CoCl_2$	401.3	108.0	40.1	78.8
13	g-C_3N_4-$CoCl_2$	20.9	454.5	2.1	4.4
14	g-C_3N_4-bulky-30	1482.4	196.5	148.2	88.3

[a] Reaction conditions: 2.0 mg catalyst, CH_3CN/H_2O/TEOA ($v/v/v$ = 3:1:1), 15.0 mg 2,2′-bpy, Xe lamp (300 W, $\lambda > 420$ nm), 10 h, 25 °C. b: Ar atmosphere, c: without catalyst; d: without TEOA; e: without light.

gas was detected during the catalytic reaction processes (Table 1, Entry 6–8), which indicate that the catalyst, sacrificial reductant and light irradiation are all indispensible to CO_2-to-CO conversion. In addition, we found that the volume ratio of CH_3CN/H_2O also affects the catalyst efficiency. As shown in Fig. S12, CH_3CN/H_2O with volume ratio of 3:1 is the improved solvent system, where g-C_3N_4-MOLs-30 exhibits the best catalytic efficiency for photochemical CO_2 reduction.

To well understand the excellent activity of g-C_3N_4-MOLs-30, several control experiments of photochemical CO_2 reduction were performed (Table 1, Entry 9–14; Fig. 3b). Firstly, bare g-C_3N_4 and Co-MOLs were used as the catalysts to photochemical CO_2 reduction, respectively. As shown in Table 1, neither g-C_3N_4 nor Co-MOLs could catalyze the photochemical CO_2 reduction reaction, as no CO production was observed during the catalytic process (Table 1, Entry 9–10; Fig. 3b). Secondly, the physical mixture of g-C_3N_4&$CoCl_2$ and g-C_3N_4&Co-MOLs were employed as the catalysts, respectively. Only negligible amount of CO and H_2 was detected, and the generated CO was much lower than that by g-C_3N_4-MOLs-30 (Table 1, Entry 11–12; Fig. 3b), indicating that the immobilization of Co(II) on g-C_3N_4 is significant for enhance its activity for photocatalytic CO_2 reduction. Thirdly, $CoCl_2$ was used as the cobalt source precursor instead of Co-MOLs to synthesize Co sites depositing g-C_3N_4 catalyst. The results show that with the same cobalt loading, the amount of CO produced by g-C_3N_4-$CoCl_2$ was also much lower than that of g-C_3N_4-MOLs-30 (Table 1, Entry 13; Fig. 3b). The lower activity of g-C_3N_4-$CoCl_2$ may be attributed to the aggregation of the active sites, as the TEM images of g-C_3N_4-$CoCl_2$ showed some metal nanoparticles with size of about 8.0 nm on g-C_3N_4, while none was detected for g-C_3N_4-MOLs-30 (Fig. S13). This results demonstrate that the order structure and the confined Co(II) in the cobalt source precursor is important to enhance its catalytic activity. Finally, the bulky Co-MOF was used as cobalt source precursor instead of Co-MOLs, the result shows only 2.96 μmol CO and 0.39 μmol H_2 were produced under the same conditions, corresponding to the CO generated rate of 148.2 $\mu mol \cdot g^{-1} \cdot h^{-1}$ (Table 1, Entry 14; Fig. 3b). This value is also much lower than that of g-C_3N_4-MOLs-30 (464.1 $\mu mol \cdot g^{-1} \cdot h^{-1}$; Table 1, Entry 3), indicating that MOLs benefit to form g-C_3N_4-based catalyst with enhanced catalytic activity. All the results of above control experiments and characterization highlight that the MOLs are the optimal cobalt source precursors for the preparation of g-C_3N_4-based catalysts for photochemical CO_2 reduction, and the pyrolysis of ultrathin Co-MOLs during the process of C_3N_4 formation is a key procedure for immobilizing Co(II) catalytic sites on g-C_3N_4 to get excellent CO_2 reduction photocatalysts.

In order to further confirm the excellent photocatalytic activity of g-C_3N_4-MOLs-30, we conducted the photocatalytic CO_2 reduction reaction under a low CO_2 concentration. A mixed gas containing 10% CO_2 and 90% Ar was employed to replace pure CO_2. It was found that g-C_3N_4-MOLs-30 also shows good activity, with 768.6 μmol g^{-1} of CO produced in 10 h irradiation (Fig. S14), suggesting that g-C_3N_4-MOLs-30 really possesses excellent activity for photocatalytic CO_2-to-CO conversion. To reveal the catalytically active sites, the experiments of photocatalytic CO_2 reduction by g-C_3N_4-MOLs-30 were carried out in the absence and presence of KSCN firstly. As shown in Fig. S15, a striking activity decrease of the catalytic system was observed in the presence of KSCN, indicating that the Co(II) sites are the catalytic centers in g-C_3N_4-MOLs-30. Besides activity, g-C_3N_4-MOLs-30 also has high durability during the photochemical reaction. As shown in Fig. S16, g-C_3N_4-MOLs-30 can retain high activity after three runs of photocatalytic CO_2 reduction. The structure of g-C_3N_4-MOLs-30 after photocatalysis can also keep stable (Fig. S17), and no aggregation of Co centers is observed in TEM images (Fig. S18). Moreover, the Co(II) content of g-C_3N_4-MOLs-30 after photocatalytic reaction is similar to that of freshly prepared sample (Table S1). These results demonstrate that g-C_3N_4-MOLs-30 really possesses good stability during photocatalytic CO_2-to-CO conversion.

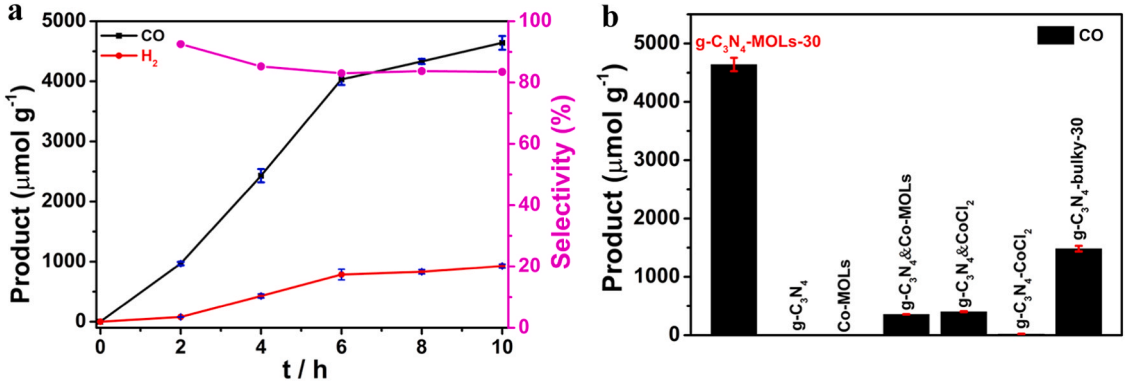

Fig. 3. Photochemical CO_2 reduction by g-C_3N_4-based catalysts. a, Time-dependent CO and H_2 generation over g-C_3N_4-MOLs-30. b, CO evolution with g-C_3N_4-MOLs-30 and other g-C_3N_4-based catalysts tested. Reaction conditions: 2.0 mg catalyst, CH_3CN/H_2O/TEOA ($v/v/v$ = 3:1:1), 15.0 mg 2,2′-bpy, Xe lamp (300 W, $\lambda > 420$ nm), 10 h, 25 °C.

2.3. Catalytic mechanism

The CO_2 adsorption tests showed that all g-C_3N_4-MOLs-X have superior CO_2 uptake than g-C_3N_4 at 298 K, and with the increase of the Co content in g-C_3N_4-MOLs-X, the CO_2 uptake remarkably increases (Fig. S19). This observation suggests that the Co(II) sites in g-C_3N_4 contribute to the CO_2 binding. The UV–vis absorption spectra of g-C_3N_4-MOLs-X exhibit obvious improvements in visible-light absorption of g-C_3N_4-MOLs-X catalysts with the increase of the amount of Co-MOLs used in g-C_3N_4 formation (Fig. 4a), illustrating that the Co(II) implantation benefits to enhance the optical performance of g-C_3N_4. The photoluminescence (PL) spectra of g-C_3N_4-MOLs-X catalysts, especially for g-C_3N_4-MOLs-30/40, show significantly damped emission in contrast to pristine g-C_3N_4 (Fig. 4b), indicating more efficient charge separation of g-C_3N_4-MOLs-X catalysts than pristine g-C_3N_4. Moreover, the time-resolved photoluminescence (TRPL) spectra revealed a reduced average exciton lifetime of 3.82 ns for g-C_3N_4 to 1.93 ns for g-C_3N_4-MOLs-30, also illustrating that the introduction of atomically dispersed Co(II) sites on g-C_3N_4 significantly accelerates the charge transfer (Fig. 4c).

The good catalytic performance of g-C_3N_4-MOLs-X was further revealed by electrochemical method. Cyclic voltammetry (CV) and linear sweep voltammetry (LSV) measurements of g-C_3N_4-MOLs-30 showed that g-C_3N_4-MOLs-30 has a larger current in CO_2 atmosphere than in Ar atmosphere (Fig. S20), indicating that g-C_3N_4-MOLs-30 has a good combination and catalytic performance for CO_2. Photocurrent response tests generated a remarkably increased photocurrent of g-C_3N_4-MOLs-30 upon light irradiation, about 2.5 times larger than that of g-C_3N_4 (Fig. 4d), confirming the better separation efficiency of photo-induced electrons in g-C_3N_4-MOLs-30 over g-C_3N_4. Electrochemical impedance measurements showed that in the Nyquist plots, a smaller diameter of capacitive loop for g-C_3N_4-MOLs-30 was observed in

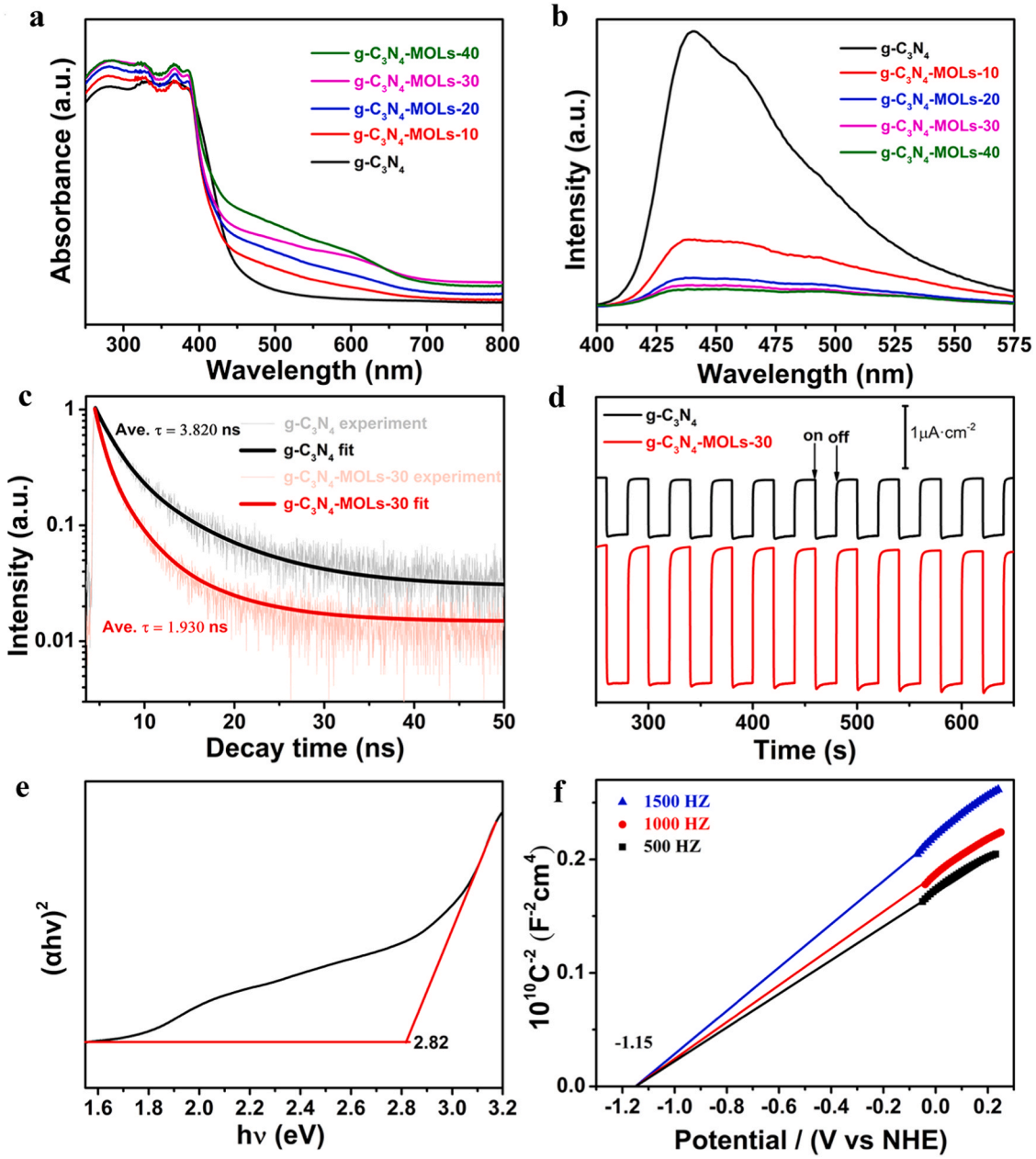

Fig. 4. Mechanistic studies of g-C_3N_4-MOLs-30 in photochemical CO_2 reduction. a, UV–vis absorption spectra of g-C_3N_4-MOLs-X. b, PL spectra of g-C_3N_4-MOLs-X screened at room temperature. c, Time-resolved photoluminescence decays of g-C_3N_4 and g-C_3N_4-MOLs-30. d, Photocurrent response of g-C_3N_4 and g-C_3N_4-MOLs-30. e, Plots of $(\alpha h\upsilon)^2$ versus energy ($h\upsilon$) for the band gap energies of g-C_3N_4-MOLs-30. f, Mott−Schottky plots of g-C_3N_4-MOLs-30.

contrast to g-C_3N_4 (Fig. S21), also illustrating that the electrons of g-C_3N_4-MOLs-30 transfer more easily than those of g-C_3N_4. By Tauc plots, the band gaps (E_g) of g-C_3N_4 and g-C_3N_4-MOLs-30 were calculated to be 2.61 and 2.82 eV vs. NHE, respectively (Fig. 4e and S22a). By Mott-Schottky plots, the conduction band (CB) potentials of g-C_3N_4 and g-C_3N_4-MOLs-30 were determined to be −1.26 and −1.15 eV vs. NHE, respectively (Fig. 4f and S22b). Thus combined UV–vis result with Mott-Schottky plot, the valence band (VB) potential of g-C_3N_4 and g-C_3N_4-MOLs-30 can be calculated to be 1.35 and 1.65 eV vs. NHE, respectively (Fig. S23). Obviously, the CB potential of g-C_3N_4 and g-C_3N_4-MOLs-30 are more negative than the redox potential of photocatalytic reduction of CO_2 to CO (−0.53 V vs. NHE) [29]. Therefore, g-C_3N_4 and g-C_3N_4-MOLs-30 could theoretically serve as photocatalyst to perform CO_2 reduction. Based on the above results, the photocatalytic mechanism of g-C_3N_4-MOLs-30 for CO_2 reduction was proposed and schematically illustrated in Fig. S24. Upon visible-light irradiation, electrons are promoted from the valence band of g-C_3N_4 to its corresponding conduction band. The photogenerated electrons migrate to the surface of g-C_3N_4 and then transfer to Co(II) active centers, where the adsorbed CO_2 molecules get electrons and are reduced to CO simultaneously. The holes that remained within the valence band of g-C_3N_4 are consumed by the electron donor TEOA.

3. Discussion

To summarize, first of all, we in large scale prepared an 2D ultrathin Co-MOLs from 3D bulky Co-MOF by our previously developed ligand replacement approach [67]. Then by pyrolysis of ultrathin Co-MOLs during the process of C_3N_4 formation, we successfully transferred and anchored the Co(II) sites on C_3N_4 to obtain a series of single Co(II) sites anchoring g-C_3N_4 catalysts (g-C_3N_4-MOLs-X). With g-C_3N_4-MOLs-X as photocatalysts, triethanolamine (TEOA) as sacrificial reductant, and CH_3CN/H_2O as reaction media, efficient and economic catalytic systems for photochemical CO_2-to-CO conversion were built. The g-C_3N_4-MOLs-30 shows the highest catalytic efficiency, with the CO generation rate of 464.1 $\mu mol \cdot g^{-1} \cdot h^{-1}$, highest among those of reported C_3N_4-based photocatalysts (Table S3). This work paves a new way to develop simple and cheap photocatalytic systems for energy conversion.

4. Methods

4.1. Synthesis of Co-MOLs

30 mg of bulky Co-MOF was dispersed in 15 mL DMSO and ultrasonicated for 10 h, a pink clear solution was obtained. The solution was concentrated at 100 °C. Pink powder was formed and collected. The powder was washed with methanol for five times and dried in a vacuum oven at 60 °C.

4.2. Synthesis of g-C_3N_4-MOLs-X

5 g urea and Co-MOLs (10, 20, 30 or 40 mg) were mixed uniformly in a covered crucible, and then heated at 550 °C for 4 h under air. The obtained powder was washed by deionized water and ethanol, and then dried in a vacuum oven at 60 °C for 24 h.

4.3. Synthesis of g-C_3N_4-bulky-30 and g-C_3N_4-$CoCl_2$

The procedures for preparing g-C_3N_4-bulky-30 and g-C_3N_4-$CoCl_2$ were similar to that of g-C_3N_4-MOLs-X, except using bulky Co-MOF (30 mg) or $CoCl_2 0.6\ H_2O$ (19 mg) instead of Co-MOLs.

4.4. Synthesis of g-C_3N_4

g-C_3N_4 was synthesized with a similar procedure to g-C_3N_4-MOLs-X in the absence of Co-MOLs.

4.5. Photocatalytic CO_2 reduction

Typically, 2 mg catalyst and 15 mg 2,2′-bipyridine were dispersed/dissolved in 5.0 mL CH_3CN/H_2O/TEOA ($v/v/v$ = 3:1:1) solution in a 17.5 mL quartz test tube. The mixture was bubbled with argon for 30 min and then with CO_2 for another 30 min under stirring. The photocatalytic reaction was initiated upon irradiation by a 300 W Xe lamp with a 420 nm cutoff filter. The generated gaseous and liquid products were detected and quantified with a gas chromatography and an ion chromatograph, respectively. Each photocatalytic reaction was repeated for at least three times to ensure the reliability of the data.

CRediT authorship contribution statement

D.C.Z conceived and designed the project, J.H.Z and W.Y performed the experiments, J.H.Z, M.Z, H.J.W, R.S, D.C.Z and T.B.L analyzed the data, J.H.Z, H.J.W, R.S and D.C.Z wrote and revised the article.

Declaration of Competing Interest

The authors declare that they have no known competing financial interests or personal relationships that could have appeared to influence the work reported in this paper.

Acknowledgments

This work was supported by the National Key Research and Development Program of China (2017YFA0700104), the National Natural Science Foundation of China (22071182, 21931007, 21861001, 21903060 and 21790052), 111 Project of China (D17003), the Natural Science Foundation of Tianjin City (17JCJQJC43800), and the Science and Technology Development Fund of Tianjin Education Commission for Higher Education (2018KJ129).

Appendix A. Supporting information

Supplementary data associated with this article can be found in the online version at doi:10.1016/j.nanoen.2020.105542.

References

[1] J.L. Qiao, Y.Y. Liu, F. Hong, J.J. Zhang, A review of catalysts for the electroreduction of carbon dioxide to produce low-carbon fuels, Chem. Soc. Rev. 43 (2014) 631–675.
[2] C.G. Bell, F. Gao, W. Yuan, L. Roos, R.J. Acton, Y. Xia, J. Bell, K. Ward, M. Mangino, P.G. Hysi, J. Wang, T.D. Spector, Oriented electron transmission in polyoxometalate-metalloporphyrin organic framework for highly selective electroreduction of CO_2, Nat. Commun. 9 (2018) 8.
[3] J.L. White, M.F. Baruch, J.E. Pander, Y. Hu, I.C. Fortmeyer, J.E. Park, T. Zhang, K. Liao, J. Gu, Y. Yan, T.W. Shaw, E. Abelev, A.B. Bocarsly, Light-driven heterogeneous reduction of carbon dioxide: photocatalysts and photoelectrodes, Chem. Rev. 115 (2015) 12888–12935.
[4] P.D. Tran, L.H. Wong, J. Barber, J.S.C. Loo, Recent advances in hybrid photocatalysts for solar fuel production, Energy Environ. Sci. 5 (2012) 5902–5918.
[5] T. Ouyang, H.H. Huang, J.W. Wang, D.C. Zhong, T.B. Lu, A dinuclear cobalt cryptate as a homogeneous photocatalyst for highly selective and efficient visible-light driven CO_2 reduction to CO in CH_3CN/H_2O solution, Angew. Chem. Int. Ed. 56 (2017) 738–743.
[6] F. Studt, I. Sharafutdinov, F. Abild-Pedersen, C.F. Elkjaer, J.S. Hummelshoj, S. Dahl, I. Chorkendorff, J.K. Norskov, Discovery of a Ni-Ga catalyst for carbon dioxide reduction to methanol, Nat. Chem. 6 (2014) 320–324.
[7] L. Liang, X.D. Li, Y.F. Sun, Y.L. Tan, X.C. Jiao, H.X. Ju, Z.M. Qi, J.F. Zhu, Y. Xie, Infrared light-driven CO_2 overall splitting at room temperature, Joule 2 (2018) 1004–1016.
[8] K.Y. Niu, Y. Xu, H.C. Wang, R. Ye, H.L. Xin, F. Lin, C.X. Tian, Y.W. Lum, K. C. Bustillo, M.M. Doeff, M.T.M. Koper, J. Ager, R. Xu, H.M. Zheng, A spongy nickel-organic CO_2 reduction photocatalyst for nearly 100% selective CO production, Sci. Adv. 3 (2017), e1700921.
[9] L.Z. Dong, L. Zhang, J. Liu, Q. Huang, M. Lu, W.X. Ji, Y.Q. Lan, Stable heterometallic cluster-based organic framework catalysts for artificial photosynthesis, Angew. Chem. Int. Ed. 59 (2020) 2659–2663.

[10] H.Q. Xu, J. Hu, D. Wang, Z. Li, Q. Zhang, Y. Luo, S.H. Yu, H.L. Jiang, Visible-light photoreduction of CO_2 in a metal-organic framework: boosting electron-hole separation via electron trap states, J. Am. Chem. Soc. 137 (2015) 13440–13443.

[11] Y.Z. Zhang, B.Q. Xia, J.R. Ran, K. Davey, S.Z. Qiao, Atomic-level reactive sites for semiconductor-based photocatalytic CO_2 reduction, Adv. Energy Mater. 10 (2020) 23.

[12] D.L. Liu, Y. Xu, M.Y. Sun, Y. Huang, Y.F. Yu, B. Zhang, Photothermally assisted photocatalytic conversion of CO_2-H_2O into fuels over a WN-WO_3 Z-scheme heterostructure, J. Mater. Chem. A 8 (2020) 1077–1083.

[13] J.W. Wang, W.J. Liu, D.C. Zhong, T.B. Lu, Nickel complexes as molecular catalysts for water splitting and CO_2 reduction, Coord. Chem. Rev. 378 (2019) 237–261.

[14] S.Y. Wang, X. Hai, X. Ding, S.B. Jin, Y.G. Xiang, P. Wang, B. Jiang, F. Ichihara, M. Oshikiri, X.G. Meng, Y.X. Li, W. Matsuda, J. Ma, S. Seki, X.P. Wang, H. Huang, Y. Wada, H. Chen, J.H. Ye, Intermolecular cascaded pi-conjugation channels for electron delivery powering CO_2 photoreduction, Nat. Commun. 11 (2020) 1149.

[15] T. Ouyang, H.J. Wang, H.H. Huang, J.W. Wang, S. Guo, W.J. Liu, D.C. Zhong, T. B. Lu, Dinuclear metal synergistic catalysis boosts photochemical CO_2-to-CO conversion, Angew. Chem. Int. Ed. 57 (2018) 16480–16485.

[16] J. Bonin, M. Robert, M. Routier, Selective and efficient photocatalytic CO_2 reduction to CO using visible light and an iron-based homogeneous catalyst, J. Am. Chem. Soc. 136 (2014) 16768–16771.

[17] D.C. Liu, T. Ouyang, R. Xiao, W.J. Liu, D.C. Zhong, Z.T. Xu, T.B. Lu, Anchoring Co^{II} Ions into a thiol-laced metal-organic framework for efficient visible-light-driven conversion of CO_2 into CO, ChemSusChem 12 (2019) 2166–2170.

[18] U. Ulmer, T. Dingle, P.N. Duchesne, R.H. Morris, A. Tayasoli, T. Wood, G.A. Ozin, Fundamentals and applications of photocatalytic CO_2 methanation, Nat. Commun. 10 (2019) 3169.

[19] H. Rao, L.C.S. Chmidt, J. Bonin, M. Robert, Visible-light-driven methane formation from CO_2 with a molecular iron catalyst, Nature 548 (2017) 74–77.

[20] M.A.A. Aziz, A.A. Jalil, S. Triwahyono, A. Ahmad, CO_2 methanation over heterogeneous catalysts: recent progress and future prospects, Green. Chem. 17 (2015) 2647–2663.

[21] R. Long, Y. Li, Y. Liu, S. Chen, X. Zheng, C. Gao, C. He, N. Chen, Z. Qi, L. Song, J. Jiang, J. Zhu, Y. Xiong, Isolation of Cu atoms in Pd lattice: forming highly selective sites for photocatalytic conversion of CO_2 to CH_4, J. Am. Chem. Soc. 139 (2017) 4486–4492.

[22] Z. Chen, M.R. Gao, Y.Q. Zhang, N. Duan, T. Fan, J. Xiao, J. Zhang, Y. Dong, J. Li, X. Yi, J.L. Luo, Tuning local carbon active sites saturability of graphitic carbon nitride to boost CO_2 electroreduction towards CH_4, Nano Energy 73 (2020), 104833.

[23] R. Kuriki, K. Sekizawa, O. Ishitani, K. Maeda, Visible-light-driven CO_2 reduction with carbon nitride: enhancing the activity of ruthenium catalysts, Angew. Chem. Int. Ed. 54 (2015) 2406–2409.

[24] D.K. Wang, R.K. Huang, W.J. Liu, D.R. Sun, Z.H. Li, Fe-based MOFs for photocatalytic CO_2 reduction: role of coordination unsaturated sites and dual excitation pathways, ACS Catal. 4 (2014) 4254–4260.

[25] E.B. Cole, P.S. Lakkaraju, D.M. Rampulla, A.J. Morris, E. Abelev, A.B. Bocarsly, Using a one-electron shuttle for the multielectron reduction of CO_2 to methanol: kinetic, mechanistic, and structural insights, J. Am. Chem. Soc. 132 (2010) 11539–11551.

[26] Y.A. Wu, I. McNulty, C. Liu, K.C. Lau, Q. Liu, A.P. Paulikas, C.J. Sun, Z.H. Cai, J. R. Guest, Y. Ren, V. Stamenkovic, L.A. Curtiss, Y.Z. Liu, T. Rajh, Facet-dependent active sites of a single Cu_2O particle photocatalyst for CO_2 reduction to methanol, Nat. Energy 4 (2019) 957–968.

[27] L.Z. Zeng, Z.Y. Wang, Y.K. Wang, J. Wang, Y. Guo, H.H. Hu, X.F. He, C. Wang, W. B. Lin, Photoactivation of Cu centers in metal-organic frameworks for selective CO_2 conversion to ethanol, J. Am. Chem. Soc. 142 (2020) 75–79.

[28] A. Alvarez, A. Bansode, A. Urakawa, A.V. Bavykina, T.A. Wezendonk, M. Makkee, J. Gascon, F. Kapteijn, Challenges in the greener production of formates/formic acid, methanol, and DME by heterogeneously catalyzed CO_2 hydrogenation processes, Chem. Rev. 117 (2017) 9804–9838.

[29] D.C. Liu, D.C. Zhong, T.B. Lu, Non-noble metal-based molecular complexes for CO_2 reduction: from the ligand design perspective, EnergyChem 2 (2020) 10034.

[30] S.N. Talapaneni, G. Singh, I.Y. Kim, K. AlBahily, Aa.H. Al-Muhtaseb, A.S. Karakoti, E. Tavakkoli, A. Vinu, Nanostructured carbon nitrides for CO_2 capture and conversion, Adv. Mater. 32 (2020), 1904635.

[31] J.H. Deng, J. Luo, Y.L. Mao, S. Lai, Y.N. Gong, D.C. Zhong, T.B. Lu, π-π stacking interactions: non-negligible forces for stabilizing porous supramolecular frameworks, Sci. Adv. 6 (2020) eaax9976, eaax9976.

[32] J.W. Wang, D.C. Zhong, T.B. Lu, Artificial photosynthesis: catalytic water oxidation and CO_2 reduction by dinuclear non-noble-metal molecular catalysts, Coord. Chem. Rev. 377 (2018) 225–236.

[33] B. Han, X.W. Ou, Z.Q. Deng, Y. Song, C. Tian, H. Deng, Y.J. Xu, Z. Lin, Nickel metal-organic framework monolayers for photoreduction of diluted CO_2 : metal-node-dependent activity and selectivity, Angew. Chem. Int. Ed. 57 (2018) 16811–16815.

[34] X. Wang, K. Maeda, A. Thomas, K. Takanabe, G. Xin, J.M. Carlsson, K. Domen, M. Antonietti, A metal-free polymeric photocatalyst for hydrogen production from water under visible light, Nat. Mater. 8 (2009) 76–80.

[35] J. Zhang, Y. Chen, X. Wang, Two-dimensional covalent carbon nitride nanosheets: synthesis, functionalization, and applications, Energy Environ. Sci. 8 (2015) 3092–3108.

[36] Z. Fang, Y. Bai, L. Li, D. Li, Y. Huang, R. Chen, W. Fan, W. Shi, In situ constructing intramolecular ternary homojunction of carbon nitride for efficient photoinduced molecular oxygen activation and hydrogen evolution, Nano Energy 75 (2020), 104865.

[37] G. Zhang, J. Zhang, M. Zhang, X. Wang, Polycondensation of thiourea into carbon nitride semiconductors as visible light photocatalysts, J. Mater. Chem. 22 (2012) 8083–8091.

[38] S.C. Yan, Z.S. Li, Z.G. Zou, Photodegradation performance of g-C_3N_4 fabricated by directly heating melamine, Langmuir 25 (2009) 10397–10401.

[39] H. Wang, X. Yuan, Y. Wu, G. Zeng, X. Chen, L. Leng, H. Li, Synthesis and applications of novel graphitic carbon nitride/metal-organic frameworks mesoporous photocatalyst for dyes removal, Appl. Catal. B-Environ. 174 (2015) 445–454.

[40] Z. Chen, E. Vorobyeva, S. Mitchell, E. Fako, N. Lopez, S.M. Collins, R.K. Leary, P. A. Midgley, R. Hauert, J. Perez-Ramirez, Single-atom heterogeneous catalysts based on distinct carbon nitride scaffolds, Natl. Sci. Rev. 5 (2018) 642–652.

[41] Y. Fang, X. Wang, Photocatalytic CO_2 conversion by polymeric carbon nitrides, Chem. Commun. 54 (2018) 5674–5687.

[42] W.J. Ong, L.L. Tan, Y.H. Ng, S.T. Yong, S.P. Chai, Graphitic carbon nitride (g-C_3N_4)-based photocatalysts for artificial photosynthesis and environmental remediation: are we a step closer to achieving sustainability? Chem. Rev. 116 (2016) 7159–7329.

[43] S. Roy, E. Reisner, Visible-light-driven CO_2 reduction by mesoporous carbon nitride modified with polymeric cobalt phthalocyanine, Angew. Chem. Int. Ed. 58 (2019) 12180–12184.

[44] R. Kuriki, M. Yamamoto, K. Higuchi, Y. Yamamoto, M. Akatsuka, D. Lu, S. Yagi, T. Yoshida, O. Ishitani, K. Maeda, Robust binding between carbon nitride nanosheets and a binuclear ruthenium(II) complex enabling durable, selective CO_2 reduction under visible light in aqueous solution, Angew. Chem. Int. Ed. 56 (2017) 4867–4871.

[45] C. Cometto, R. Kuriki, L. Chen, K. Maeda, T.-C. Lau, O. Ishitani, M. Robert, A carbon nitride/Fe quaterpyridine catalytic system for photostimulated CO_2-to-CO conversion with visible light, J. Am. Chem. Soc. 140 (2018) 7437–7440.

[46] Z. Jiang, W. Wan, H. Li, S. Yuan, H. Zhao, P.K. Wong, A hierarchical Z-scheme α-Fe_2O_3/g-C_3N_4 hybrid for enhanced photocatalytic CO_2 reduction, Adv. Mater. 30 (2018), 1706108.

[47] M. Ou, W. Tu, S. Yin, W. Xing, S. Wu, H. Wang, S. Wan, Q. Zhong, R. Xu, Amino-assisted anchoring of $CsPbBr_3$ perovskite quantum dots on porous g-C_3N_4 for enhanced photocatalytic CO_2 reduction, Angew. Chem. Int. Ed. 57 (2018) 13570–13574.

[48] B. Ma, G. Chen, C. Fave, L. Chen, R. Kuriki, K. Maeda, O. Ishitani, T.C. Lau, J. Bonin, M. Robert, Efficient visible-light-driven CO_2 reduction by a cobalt molecular catalyst covalently linked to mesoporous carbon nitride, J. Am. Chem. Soc. 142 (2020) 6188–6195.

[49] G. Vilé, D. Albani, M. Nachtegaal, Z.P. Chen, D. Dontsova, M. Antonietti, N. Lopez, J. Perez-Ramirez, A stable single-site palladium catalyst for hydrogenations, Angew. Chem. Int. Ed. 54 (2015) 11265–11269.

[50] X.G. Li, W.T. Bi, L. Zhang, S. Tao, W.S. Chu, Q. Zhang, Y. Luo, C.Z. Wu, Y. Xie, Single-atom Pt as co-catalyst for enhanced photocatalytic H_2 evolution, Adv. Mater. 28 (2016) 2427–2431.

[51] W. Liu, L.L. Cao, W.R. Cheng, Y.J. Cao, X.K. Liu, W. Zhang, X.L. Mou, L.L. Jin, X. S. Zheng, W. Che, Q.H. Liu, T. Yao, S.Q. Wei, Single-site active cobalt-based photocatalyst with a long carrier lifetime for spontaneous overall water splitting, Angew. Chem. Int. Ed. 56 (2017) 9312–9317.

[52] P. Huang, J. Huang, S.A. Pantovich, A.D. Carl, T.G. Fenton, C.A. Caputo, R. L. Grimm, A.I. Frenkel, G. Li, Selective CO_2 reduction catalyzed by single cobalt sites on carbon nitride under visible-light irradiation, J. Am. Chem. Soc. 140 (2018) 16042–16047.

[53] S.B. Tian, Z.Y. Wang, W.B. Gong, W.X. Chen, Q.C. Feng, Q. Wu, C. Chen, C. Chen, Q. Peng, L. Gu, H.J. Zhao, P. Hu, D.S. Wang, Y.D. Li, Temperature-controlled selectivity of hydrogenation and hydrodeoxygenation in the conversion of biomass molecule by the Ru-1/mpg-C_3N_4 catalyst, J. Am. Chem. Soc. 140 (2018) 11161–11164.

[54] Y.J. Cao, S. Chen, Q.Q. Luo, H. Yan, Y. Lin, W. Liu, L.L. Cao, J.L. Lu, J.L. Yang, T. Yao, S.Q. Wei, Atomic-level insight into optimizing the hydrogen evolution pathway over a Co_1-N_4 single-site photocatalyst, Angew. Chem. Int. Ed. 56 (2017) 12191–12196.

[55] Y.R. Li, Z.W. Wang, T. Xia, H.X. Ju, K. Zhang, R. Long, Q. Xu, C.M. Wang, L. Song, J.F. Zhu, J. Jiang, Y.J. Xiong, Implementing metal-to-ligand charge transfer in organic semiconductor for improved visible-near-infrared photocatalysis, Adv. Mater. 28 (2016) 6959–6965.

[56] Z.P. Chen, S. Mitchell, E. Vorobyeva, R.K. Leary, R. Hauert, T. Furnival, Q. M. Ramasse, J.M. Thomas, P.A. Midgley, D. Dontsova, M. Antonietti, S. Pogodin, N. Lopez, J. Perez-Ramirez, Stabilization of single metal atoms on graphitic carbon nitride, Adv. Funct. Mater. 27 (2017), 1605785.

[57] Y. Guo, W.J. Shi, H.J. Yang, Q.F. He, Z.M. Zeng, J.Y. Ye, X.R. He, R.Y. Huang, C. Wang, W.B. Lin, Cooperative stabilization of the [pyridinium-CO_2-Co] adduct on a metal-organic layer enhances electrocatalytic CO_2 reduction, J. Am. Chem. Soc. 141 (2019) 17875–17883.

[58] M.T. Zhao, Q.P. Lu, Q.L. Ma, H. Zhang, Two-dimensional metal-organic framework nanosheets, Small Methods 1 (2017) 8.

[59] J.G. Duan, Y.S. Li, Y.C. Pan, N. Behera, W.Q. Jin, Metal-organic framework nanosheets: an emerging family of multifunctional 2D materials, Coord. Chem. Rev. 395 (2019) 25–45.

[60] S.C. Junggeburth, L. Diehl, S. Werner, V. Duppel, W. Sigle, B.V. Lotsch, Ultrathin 2D coordination polymer nanosheets by surfactant-mediated synthesis, J. Am. Chem. Soc. 135 (2013) 6157–6164.

[61] Y. Wang, M. Zhao, J. Ping, B. Chen, X. Cao, Y. Huang, C. Tan, Q. Ma, S. Wu, Y. Yu, Q. Lu, J. Chen, W. Zhao, Y. Ying, H. Zhang, Bioinspired design of ultrathin 2D

bimetallic metal-organic-framework nanosheets used as biomimetic enzymes, Adv. Mater. 28 (2016) 4149–4155.
[62] X. Huang, P. Sheng, Z. Tu, F. Zhang, J. Wang, H. Geng, Y. Zou, C.-a Di, Y. Yi, Y. Sun, W. Xu, D. Zhu, A two-dimensional pi-d conjugated coordination polymer with extremely high electrical conductivity and ambipolar transport behaviour, Nat. Commun. 6 (2015) 7408.
[63] M.T. Zhao, Y. Huang, Y.W. Peng, Z.Q. Huang, Q.L. Ma, H. Zhang, Two-dimensional metal−organic framework nanosheets: synthesis and applications, Chem. Soc. Rev. 47 (2018) 6267–6295.
[64] W.J. Shi, L.Y. Cao, H. Zhang, X. Zhou, B. An, Z.K. Lin, R.H. Dai, J.F. Li, C. Wang, W. B. Lin, Surface modification of two-dimensional metal-organic layers creates biomimetic catalytic microenvironments for selective oxidation, Angew. Chem. Int. Ed. 56 (2017) 9704–9709.
[65] W. Yang, H.J. Wang, R.R. Liu, C. Zhang, C. Li, D.C. Zhong, T.B. Lu, Tailoring crystal facets of metal–organic layers to enhance photocatalytic activity for CO_2 reduction, Angew. Chem. Int. Ed. (2020), https://doi.org/10.1002/anie.202011068.
[66] Y.L. Wang, D.Q. Yuan, W.H. Bi, X. Li, X.J. Li, F. Li, R. Cao, Syntheses and characterizations of two 3D cobalt−organic frameworks from 2D honeycomb building blocks, Cryst. Growth Des. 5 (2005) 1849–1855.
[67] J.H. Deng, Y.Q. Wen, J. Willman, W.J. Liu, Y.N. Gong, D.C. Zhong, T.B. Lu, H. C. Zhou, Facile exfoliation of 3D pillared metal-organic frameworks (MOFs) to produce MOF nanosheets with functionalized surfaces, Inorg. Chem. 58 (2019) 11020–11027.
[68] S. Guo, S. Zhao, X. Wu, H. Li, Y. Zhou, C. Zhu, N. Yang, X. Jiang, J. Gao, L. Bai, Y. Liu, Y. Lifshitz, S.-T. Lee, Z. Kang, A Co_3O_4-CDots-C_3N_4 three component electrocatalyst design concept for efficient and tunable CO_2 reduction to syngas, Nat. Commun. 8 (2017) 1828.
[69] X. Song, H. Zhang, Y. Yang, B. Zhang, M. Zuo, X. Cao, J. Sun, C. Lin, X. Li, Z. Jiang, Bifunctional nitrogen and cobalt codoped hollow carbon for electrochemical syngas production, Adv. Sci. 5 (2018), 1800177.
[70] X. Gao, J. Feng, D. Su, Y. Ma, G. Wang, H. Ma, J. Zhang, In-situ exfoliation of porous carbon nitride nanosheets for enhanced hydrogen evolution, Nano Energy 59 (2019) 598–609.
[71] J. Wang, T. Heil, B. Zhu, C. Tung, J. Yu, H.M. Chen, M. Antonietti, S. Cao, A single Cu-center containing enzyme-mimic enabling full photosynthesis under CO_2 reduction, ACS Nano 14 (2020) 8584–8593.

Ji-Hong Zhang obtained his B.S. and M.S. degree from Gannan Normal University in 2017 and 2020, respectively. He is now pursuing a Ph.D. in Tianjin University of Technology under the supervision of Prof. D. C. Zhong. His current research focuses on the design and synthesis of functional complexes for energy storage and conversion.

Wei Yang received his B.S. degree from Shanxi Datong University in 2014 and M.S. degree from Henan University in 2017. Currently, he is pursuing a Ph.D. in Tianjin University of Technology. His research focuses on the rational design and synthesis of 2D metal-organic layers for energy storage and conversion.

Min Zhang obtained his B.S. and Ph.D from Jilin University in 2004 and 2009, respectively. He then worked as a research assistant (2009–2011) and associate professor (2012–2016) in Changchun Institute of Applied Chemistry, Chinese Academy of Sciences. In 2017, he moved to Tianjin University of Technology, and then worked as a postdoctoral fellow at Linköping University. He is now a professor of Tianjin University of Technology. His research interest centers on material innovation, device engineering, and in-depth understanding of the charge and energy transfer processes for high-efficient photochemical conversion devices.

Hong-Juan Wang currently serves as a lecturer in the Institute for New Energy Materials and Low Carbon Technologies, Tianjin University of Technology. She obtained her B.S. in 2011 from Liaoning Normal University and Ph.D. in 2016 from Beijing Normal University. Her areas of research interest focus on the design of new materials for photocatalytic and electrocatalytic reduction reactions, such as CO_2 reduction and N_2 conversion.

Rui Si obtained his B.S. in 2001 and Ph.D. in 2006 from Peking University (Supervisor: Prof. Chun-Hua Yan and Prof. Ya-Wen Zhang). After three and half years postdoctoral fellowship at Prof. Maria Flytzani-Stephanopoulos' group (Tufts University), he joined Dr. Jose A. Rodriguez's group (Brookhaven National Laboratory) in 2009 as a research associate. In 2016, he moved to Shanghai Institute of Applied Physics, CAS (Professor) and worked at Shanghai Synchrotron Radiation Facility. His current research interests focus on the study of supported metal catalysts for new energy, as well as operando characterization techniques by the aids of synchrotron-based X-ray source.

Di-Chang Zhong obtained his B.S. in 2003 from Gannan Normal University and his M.S. in 2006 from Guangxi Normal University and Ph.D. in 2011 from the Sun Yat-Sen University. Then, he joined the faculty at Gannan Normal University and promoted to professor in 2017. He worked as a JSPS postdoctoral fellow at AIST, Japan for two years. In 2020, he moved to Tianjin University of Technology. His interests focus on the design and synthesis of molecular catalytic materials for energy storage and conversion.

Tong-Bu Lu obtained his B.S. in 1988 and Ph.D. in 1993 from Lanzhou University. After two years postdoctoral fellowship at Sun Yat-Sen University, he joined the faculty at the same university, and became a professor in 2000. He worked as a post doctor in F. Albert Cotton's group at Texas A&M University in 1998 and 2002, respectively. In 2016, he moved to Tianjin University of Technology. His current research interests focus on the study of artificial photosynthesis, including the design of homogeneous and heterogeneous catalysts for water splitting and CO_2 reduction.